

Investigation of Surface Magnetism in Systems Based on MnBi_2Te_4
Using the Magneto-Optical Kerr EffectD. A. Glazkova^{a,*}, D. A. Estyunin^a, A. S. Tarasov^{b,c}, N. N. Kosyrev^{b,d}, V. A. Komarov^{b,c}, G. S. Patrino^{b,c},
V. A. Golyashov^{a,e}, O. E. Tereshchenko^{a,e}, K. A. Kokh^{a,f}, A. V. Koroleva^a, and A. M. Shikin^a^a St. Petersburg State University, St. Petersburg, 198504 Russia^b Kirensky Institute of Physics, Federal Research Center “Krasnoyarsk Science Center of the Siberian Branch of the Russian Academy of Sciences,” Krasnoyarsk, 660036 Russia^c Institute of Engineering Physics and Radioelectronics, Siberian Federal University, Krasnoyarsk, 660041 Russia^d Krasnoyarsk State Agrarian University, Achinsk Branch, Achinsk, 662155 Russia^e Rzhanov Institute of Semiconductor Physics, Siberian Branch, Russian Academy of Sciences, Novosibirsk, 630090 Russia^f Sobolev Institute of Geology and Mineralogy, Siberian Branch, Russian Academy of Sciences, Novosibirsk, 630090 Russia

*e-mail: daria.a.glazkova@gmail.com

Received April 10, 2023; revised April 10, 2023; accepted June 8, 2023

Abstract— MnBi_2Te_4 , $\text{Mn}(\text{Bi,Sb})_2\text{Te}_4$, and $\text{MnBi}_2\text{Te}_4(\text{Bi}_2\text{Te}_3)_m$ ($m \geq 1$) are assigned to magnetic topological insulators. Successful application of these materials in nanoelectronic devices calls for comprehensive investigation of their electronic structure and magnetic properties in dependence of the Bi/Sb atomic ratio and the number m of Bi_2Te_3 blocks. The magnetic properties of the surface of MnBi_2Te_4 , MnBi_4Te_7 , and $\text{Mn}(\text{Bi}_{1-x}\text{Sb}_x)_2\text{Te}_4$ compounds ($x = 0.43$ and 0.32) have been studied using the magneto-optical Kerr effect. It is shown that the temperatures of magnetic transitions on the surface and in the bulk of MnBi_4Te_7 and $\text{Mn}(\text{Bi, Sb})_2\text{Te}_4$ differ significantly.

DOI: 10.1134/S1063774523601296

INTRODUCTION

The relationship between the electronic and magnetic properties in magnetic topological insulators (MTIs), in combination with their nontrivial topology, provides the possibility of implementing unique quantum effects, such as anomalous quantum Hall effect, axion insulator state, and Majorana fermions [1–13]. The most promising materials for observing these effects are MnBi_2Te_4 and the families of related materials: $\text{Mn}(\text{Bi,Sb})_2\text{Te}_4$ and $\text{MnBi}_2\text{Te}_4(\text{Bi}_2\text{Te}_3)_m$ [14–16]. The electronic structure of topological surface states of MnBi_2Te_4 may have an anomalously wide (in comparison with the other known MTIs) energy gap. The magnetic ordering temperature in MnBi_2Te_4 is $T_N = 24.5$ K [14] (a record-high value among the known MTIs). In view of these specific features, the MnBi_2Te_4 compound and related materials have been of great interest for the past few years [17–19]. However, the experimental data characterizing the electronic and magnetic structures of these materials differ significantly. For example, when studying the gap at

the Dirac point, values from several to tens of meV were obtained [20]. According to the data of some works, this behavior may be due to either structural defects affecting the distribution of topological surface states and their interaction with Mn atoms [21] or changes in the magnetic order (including those occurring near the surface) [22].

For MnBi_2Te_4 , A-type antiferromagnetic (AFM) ordering with magnetic moments oriented perpendicular to the (0001) surface is energetically favorable [23]. This magnetic structure is confirmed by different experimental methods: neutron diffraction study [24, 25], SQUID magnetometry [26], X-ray magnetic circular dichroism spectroscopy [14], and angle-resolved photoelectron spectroscopy (ARPES) [27]. The values of the Néel temperature measured by the surface- and bulk-sensitive methods differed very little.

However, magnetic properties near the surface may undergo changes, as compared to bulk magnetic properties. Metamagnets (including the MnBi_2Te_4 compound) are characterized by layer-by-layer magnetiza-

tion reversal in an external magnetic field [28, 29]. This behavior is caused by a decrease in the coercive force of a surface block. Thus, a particular attention should be paid to the investigation of magnetic properties near the surface.

In this paper, we report the results of studying the magnetic properties of the MnBi_2Te_4 , $\text{MnBi}_2\text{Te}_4(\text{Bi}_2\text{Te}_3)$ (i.e., MnBi_4Te_7), and $\text{Mn}(\text{Bi,Sb})_2\text{Te}_4$ materials using the magneto-optical Kerr effect (MOKE). The temperature dependence of the MOKE signal was investigated. The reference sample for analyzing the results obtained was MnBi_2Te_4 , whose magnetic properties have been thoroughly studied.

EXPERIMENTAL

Single crystals of MnBi_2Te_4 , $\text{Mn}(\text{Bi}_{1-x}\text{Sb}_x)_2\text{Te}_4$, and MnBi_4Te_7 were synthesized by the vertical Bridgman method at the Sobolev Institute of Geology and Mineralogy of the Siberian Branch of the Russian Academy of Sciences.

Magnetic properties were measured at the Resource Center “Centre for Diagnostics of Functional Materials for Medicine, Pharmacology and Nanoelectronics” of the Research Park of St. Petersburg State University using a SQUID magnetometer with a Quantum Design helium cryostat.

Measurements by the ARPES and X-ray photoelectron spectroscopy (XPS) methods were carried out at the Rzhanov Institute of Semiconductor Physics of the Siberian Branch of the Russian Academy of Sciences on an SPECS ProvenX-ARPES setup at $h\nu = 21.22$ eV for ARPES and $h\nu = 1486.7$ eV for XPS. Clean surfaces of the samples were obtained by cleaving in an ultra-high vacuum. The basic pressure in the experiment was at the level of $\sim(3-5) \times 10^{-11}$ mbar. Additional XPS measurements were performed at the Resource Center “Centre for Physical Methods of Surface Investigation” of St. Petersburg State University on an ESCALAB 250Xi setup at $h\nu = 1486.7$ eV.

The MOKE measurements were carried out using a NanoMOKE 2 setup (Durham Magneto Optics, UK) equipped with a helium cryostat (Oxford Instruments, UK), an electromagnet (magnetic field up to 3.5 kOe), and an automated micromanipulator ensuring motion of the cryostat with a sample with respect to the laser beam with a step of 1 μm . The sensitivity of the setup is about 10^{-14} emu.

RESULTS AND DISCUSSION

The ARPES (Fig. 1a) and XPS (Fig. 1b) spectra were obtained to characterize the electronic structure and elemental composition of the MnBi_2Te_4 sample under study. Figure 1a shows clearly the states of the bulk valence band and the bulk conduction band and the wide bulk band gap between (~ 200 meV). Topo-

logical surface states are located in the vicinity of the bulk band gap. This type of the electronic structure near the Fermi level with the center of the bulk band gap at the binding energy of ~ 0.25 eV is characteristic of these materials [14]. Figure 1b shows the XPS spectrum with core level peaks. The atomic concentrations of elements on the surface of the sample were estimated based on the peak intensities using the Trzhaskovskaya database of photoionization cross sections [30]. The deviation between the calculated stoichiometry and the stoichiometry specified for the growth was 1–2%, which is close to the measurement error. Thus, the composition and electronic structure of the surface of the sample under study correspond to those of a MnBi_2Te_4 crystal. The temperature dependence of the magnetic susceptibility $\chi(T)$ measured using SQUID magnetometry (Fig. 1c) also demonstrates a pattern typical of the MnBi_2Te_4 compound [31]. The measurements were carried out in a field of 1 kOe, applied parallel to the crystallographic axis c . The kink in the dependence $\chi(T)$ at 24.5 K (Fig. 1c) indicates AFM ordering below this temperature, while the sharp increase in the magnetic susceptibility (magnetization) at 15 K is characteristic of the ferromagnetic (FM) transition.

Afterwards, the dependences of the MOKE signal on the applied magnetic field $I_{\text{MOKE}}(H)$ were measured for this sample at different temperatures in the range from 4.5 to 40 K. The field with H ranging from -2 to 2 kOe was applied along the sample surface. The experimental dependence $I_{\text{MOKE}}(H)$ had an 8-like shape rather than a hysteresis loop typical of this method. The unusual shape of the signal is related to the application of the magnetic field insufficient for spin rotation (spin-flop transition) perpendicular to the easy magnetization axis in the sample (c axis of the crystal). As a result, the paramagnetic signal was actually measured, except for the temperature regions with FM ordering of a part of the samples. Nevertheless, it was shown in [32–34] that the magneto-optical signal can be used to determine the Néel temperature. In particular, the largest optical signal is due to the changes in the refractive index along the axis oriented perpendicular to the Néel vector [34], which corresponds to the chosen geometry of the experiment. To analyze changes in the obtained temperature dependences $I_{\text{MOKE}}(H)$, each dependence was put into correspondence with a numerical parameter related to the area inside the loop and the amplitude of signal variation. The resulting parameter (signal loop area normalized to the signal amplitude) depends on temperature: $S_{\text{MOKE}}(T)$ (Fig. 1d). Note that the copper plate, on which the sample was mounted, did not exhibit any changes in the parameter $S_{\text{MOKE}}(H)$ with temperature.

The $S_{\text{MOKE}}(T)$ value (Fig. 1d) changes significantly in the vicinity of $T \approx 25$ K, which corresponds to the AFM ordering temperature in MnBi_2Te_4 . For clarity,

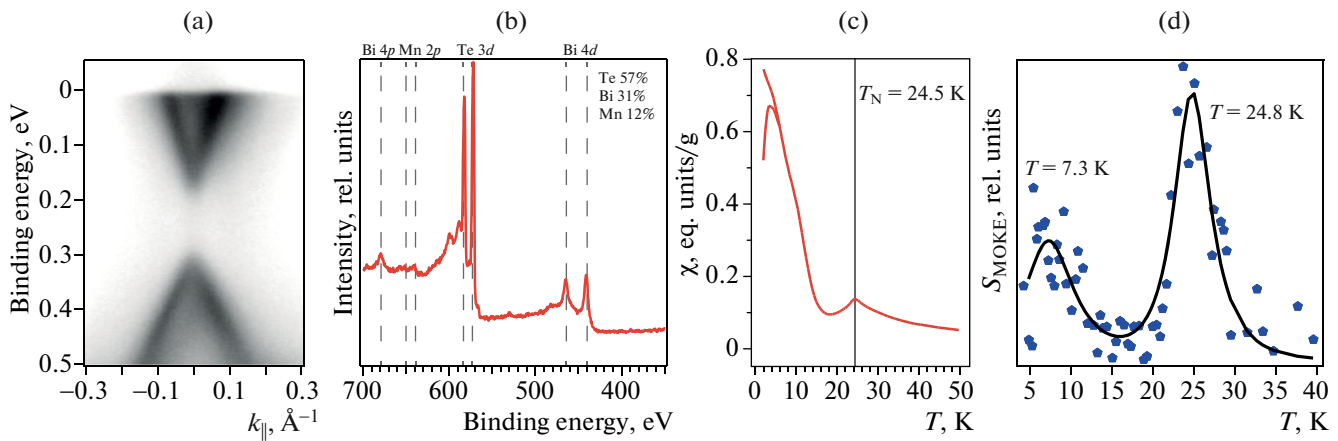


Fig. 1. MnBi_2Te_4 : (a) ARPES dispersion relation measured near the Γ point, (b) XPS spectrum of the core levels of the elements entering the sample (positions of the levels are marked by vertical lines), (c) temperature dependence of the magnetic susceptibility (AFM ordering temperature is indicated by the vertical line), and (d) dependence $S_{\text{MOKE}}(T)$ (symbols) and approximation of the signal by Gaussian peaks (solid curve).

the dependence $S_{\text{MOKE}}(T)$ is approximated by Gaussian peaks. The approximation yields the peak position at $T = 24.8$ K, which coincides (with allowance for the error) with the bulk Néel temperature. One can also see a change in the dependence $S_{\text{MOKE}}(T)$ below 10 K. The approximation of the dependence in this region by a Gaussian peak gives the temperature of $T \approx 7$ K, which is consistent with the FM transition temperature estimated from the dependence $\chi(T)$ (Fig. 1c). However, the temperature of the surface FM transition is lower than that of the bulk FM transition. Thus, the temperature ranges of peaks in the dependence $S_{\text{MOKE}}(T)$ are related to the temperatures of magnetic ordering of the system. An analysis of the dependence $S_{\text{MOKE}}(T)$ makes it possible to determine the magnetic ordering temperatures for the $\text{Mn}(\text{Bi}_{1-x}\text{Sb}_x)_2\text{Te}_4$ and MnBi_4Te_7 systems.

Figure 2a shows the ARPES dispersion relation for the MnBi_4Te_7 sample, which is typical of samples with this stoichiometry [18]. The surface of MnBi_4Te_7 samples may have two possible terminations: a quintuple-layer Bi_2Te_3 block or a septuple-layer MnBi_2Te_4 block. A mixed dispersion relation can be seen in Fig. 2a. This pattern is obtained when photoelectrons are detected from terminations of two types. The dispersion relation in Fig. 2a demonstrates the states of the bulk valence band, the bulk conduction band, and the bulk band gap between. The topological surface states are located in the bulk band gap. Figure 2b shows a full-range XPS spectrum of the MnBi_4Te_7 sample and the concentrations estimated from it. The region of the $2p$ level of Mn is also given on an enlarged scale in the inset. The sample stoichiometry corresponds to the composition of charge.

The dependence $S_{\text{MOKE}}(T)$ for the MnBi_4Te_7 sample (Fig. 2c) has two peaks at $T = 11.3$ and 21.3 K,

while the bulk Néel temperature for MnBi_4Te_7 is $T_N = 13$ K [35]. The peak at $T = 11.3$ K can be explained by the fact that the surface Néel temperature for MnBi_4Te_7 is somewhat lower than the bulk temperature. The peak at $T = 21.3$ K is characterized by a width close to that of the peak in $S_{\text{MOKE}}(T)$ for the MnBi_2Te_4 (see Fig. 1d). For the MnBi_2Te_4 and MnBi_4Te_7 samples, the peak position temperatures are also close. Thus, we can conclude that, while retaining the shapes of the electronic bands and the stoichiometry on the surface, the MnBi_4Te_7 sample may exhibit the magnetic properties of MnBi_2Te_4 . In addition, the magnetic transition temperature on the surface of the material is below the bulk Néel temperature for MnBi_2Te_4 .

The temperatures of magnetic transitions on the surface for the $\text{Mn}(\text{Bi}_{1-x}\text{Sb}_x)_2\text{Te}_4$ systems were analyzed for charge stoichiometries $x = 0.2$ and 0.3 . These Sb atomic concentrations can provide the states of the electronic structure on the crystal surfaces that are close to the compensated semiconductor state [19]. Figures 3a and 3e show the ARPES spectra of the samples; one can see that the Fermi level for the sample with the specified Sb atomic concentration of $x = 0.2$ (Fig. 3a) is located in the bulk band gap (i.e., the compensated semiconductor state is achieved). The sample with the specified Sb atomic concentration of $x = 0.3$ is in the hole doped state, and only a part of the valence band states can be seen in the dispersion relation in Fig. 3e.

The XPS spectra of the samples are presented in Figs. 3b and 3f. The Sb atomic concentrations were calculated from the peak intensities to be $x = 0.32$ and 0.43 (instead of the growth-specified values of $x = 0.2$ and 0.3 , respectively). Samples of $\text{Mn}(\text{Bi,Sb})_2\text{Te}_4$ [19, 36] are often characterized by an elevated Sb concen-

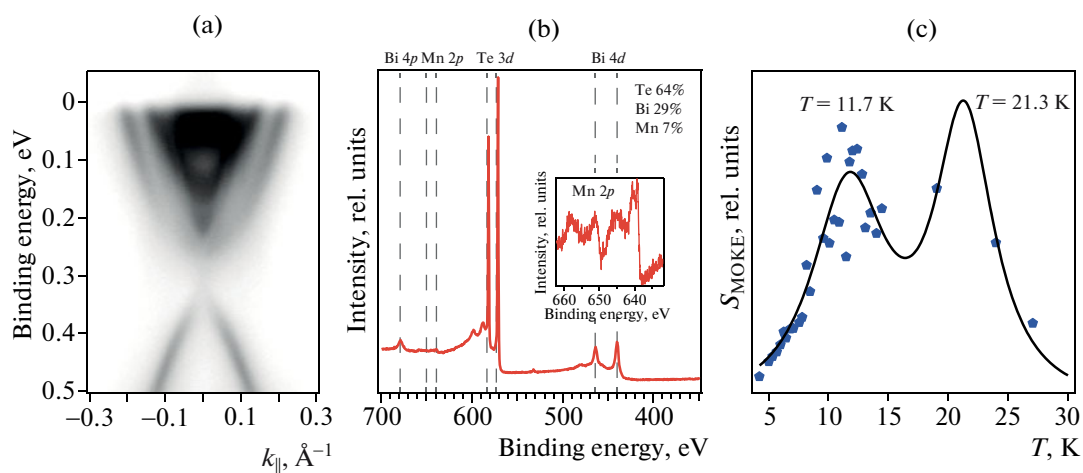


Fig. 2. MnBi_4Te_7 : (a) ARPES dispersion relation measured near the Γ point, (b) XPS spectrum of the core levels of the elements entering the sample (positions of the levels are marked by vertical lines) with the region of the $2p$ level of Mn given in the inset, and (c) dependence $S_{\text{MOKE}}(T)$ (symbols) and approximation of the signal by Gaussian peaks (solid curve).

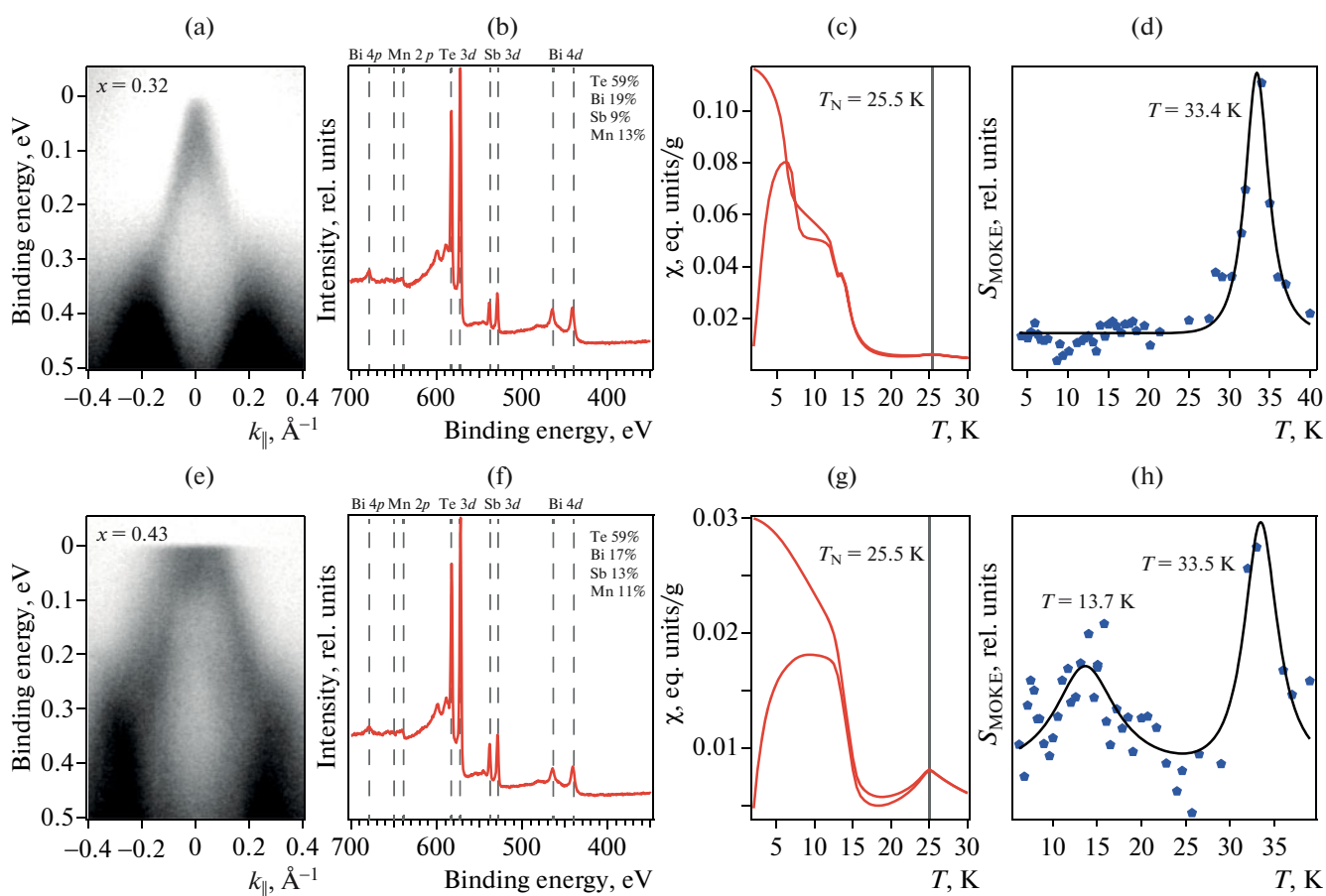


Fig. 3. $\text{Mn}(\text{Bi}_{1-x}\text{Sb}_x)_2\text{Te}_4$ at $x =$ (a–d) 0.32 and (e–h) 0.43: (a, e) ARPES dispersion relation measured near the Γ point, (b, f) XPS spectra of the core levels of the elements entering the samples (positions of the levels are marked by vertical lines), (c, g) temperature dependence of the magnetic susceptibility (AFM ordering temperature is indicated by the vertical line), and (d, h) dependence $S_{\text{MOKE}}(T)$ (symbols) and approximation of the signal by Gaussian peaks (solid curve).

tration in a crystal in comparison with the charge composition. In other respects, the samples correspond to the specified stoichiometric ratio.

The bulk magnetic properties of these materials have been widely investigated: $\text{Mn}(\text{Bi}_{1-x}\text{Sb}_x)_2\text{Te}_4$ samples at $x < 0.5$ may either exhibit purely AFM properties [37] or be in a mixed phase with simultaneous manifestation of FM and AFM properties [38]. The Néel temperature in both cases is close to $T = 24.5$ K; the Curie temperature for the second sample is ~ 17 K. Figures 3c and 3g show the temperature dependences of the magnetic susceptibility of the $\text{Mn}(\text{Bi}_{1-x}\text{Sb}_x)_2\text{Te}_4$ samples ($x = 0.32$ and 0.43) $\chi(T)$ measured using the SQUID magnetometer. The measurements were carried out in a magnetic field of 50 Oe applied along the crystallographic axis c . The magnetic susceptibility curves are characterized by the presence of the kink (typical of the AFM transition) at temperatures $T = 25.5$ K ($x = 0.32$, Fig. 3c) and $T = 25$ K ($x = 0.43$, Fig. 3g) and by the increase in $\chi(T)$ (typical of the FM transition) at a temperature of $T \approx 17$ K for both samples.

However, the magnetic transition temperature on the surface estimated by the MOKE method differs significantly from the bulk one. The dependence $S_{\text{MOKE}}(T)$ for the $\text{Mn}(\text{Bi}_{1-x}\text{Sb}_x)_2\text{Te}_4$ ($x = 0.32$) sample (Fig. 3d) contains a single peak at $T = 33.4$ K, which differs from the bulk magnetic transition temperature by approximately 8 K. Such a significant increase in the transition temperature can be caused by a change in the sample magnetic order from AFM to FM, which is due to the elevated number of Mn_{Bi} and Bi_{Mn} anti-site defects and characterized by the Curie temperature $T_C = 34$ K [39]. The fact that this temperature of the magnetic transition was not revealed in the measurements of bulk magnetic properties may be indicative of the formation of the surface by cleaving a bulk crystal with a large number of defects.

The experiment was reproduced for a sample with an increased Sb atomic concentration. The dependence $S_{\text{MOKE}}(T)$ for the $\text{Mn}(\text{Bi}_{1-x}\text{Sb}_x)_2\text{Te}_4$ ($x = 0.43$) sample (Fig. 3h) exhibits a peak of the same width, located at the same temperature (with allowance for the error). The peak at $T = 13.7$ K corresponds to the FM transition. However, the temperature of the FM transition near the surface is lower, in comparison with the SQUID data.

CONCLUSIONS

The magnetic properties of the surface of the MnBi_2Te_4 , MnBi_4Te_7 , and $\text{Mn}(\text{Bi}_{1-x}\text{Sb}_x)_2\text{Te}_4$ materials were studied by the MOKE technique. It was shown that the magnetic transition temperature can be estimated using MOKE when the external field is directed perpendicular to the magnetic moment in the sample.

It was demonstrated for the MnBi_2Te_4 samples that the temperature of the AFM transition on the surface is consistent with the bulk one, whereas the temperature of the FM transition is lower than the bulk temperature.

It was shown that there are two magnetic transitions on the MnBi_4Te_7 surface: one at the temperature corresponding to the bulk magnetic transition in MnBi_4Te_7 and the other at the temperature corresponding to the bulk magnetic transition in MnBi_2Te_4 . The temperatures of the magnetic transitions on the MnBi_4Te_7 surface are lower than those for the bulk transitions.

The analysis showed that the magnetic ordering temperatures are ~ 33 K for the $\text{Mn}(\text{Bi}_{1-x}\text{Sb}_x)_2\text{Te}_4$ ($x = 0.32$ and 0.43) materials. A possible reason is the change in the type of magnetic ordering from AFM to FM due to an increase in the number of anti-site defects in the Bi and Mn layers.

FUNDING

This study was supported by the St. Petersburg State University (project no. 94031444) and the Russian Science Foundation (grant no. 23-12-00016). The samples were synthesized within the project “State Assignment for the Sobolev Institute of Geology and Mineralogy of the Siberian Branch of the Russian Academy of Sciences and the Rzhzanov Institute of Semiconductor Physics of the Siberian Branch of the Russian Academy of Sciences.”

CONFLICT OF INTEREST

The authors of this work declare that they have no conflicts of interest.

REFERENCES

1. L. Smejkal, Y. Mokrousov, Y. Binghai, et al., *Nat. Phys.* **14**, 242 (2018).
<https://doi.org/10.1038/s41567-018-0064-5>
2. Y. Tokura, K. Yasuda, and A. Tsukazaki, *Nat. Rev. Phys.* **1**, 126 (2019).
<https://doi.org/10.1038/s42254-018-0011-5>
3. M. Z. Hasan and C. L. Kane, *Rev. Mod. Phys.* **82**, 3045 (2010).
<https://doi.org/10.1103/RevModPhys.82.3045>
4. Xiao-Liang Qi and Shou-Cheng Zhang, *Rev. Mod. Phys.* **83**, 1057 (2011).
<https://doi.org/10.1103/RevModPhys.83.1057>
5. Chao-Xing Liu, Xiao-Liang Qi, Xi Dai, et al., *Phys. Rev. Lett.* **101**, 146802 (2008).
<https://doi.org/10.1103/PhysRevLett.101.146802>
6. Rui Yu, Wei Zhang, Hai-Jun Zhang, et al., *Science* **329**, 61 (2010).
<https://doi.org/10.1126/science.1187485>
7. Cui-Zu Chang, Jinsong Zhang, Xiao Geng, et al., *Science* **340**, 167 (2013).
<https://doi.org/10.1126/science.1234414>

8. Xiao-Liang Qi, L. Hughes Taylor, Shou-Cheng Zhang, *Phys. Rev. B* **78**, 195424 (2008).
<https://doi.org/10.1103/PhysRevB.78.195424>
9. M. Mogi, M. Kawamura, R. Yoshimi, et al., *Nat. Mater.* **16**, 516 (2017).
<https://doi.org/10.1038/nmat4855>
10. Di Xiao, Jue Jiang, Jae-Ho Shin, et al., *Phys. Rev. Lett.* **120**, 056801 (2018).
<https://doi.org/10.1103/PhysRevLett.120.056801>
11. Xiangang Wan, A. M. Turner, A. Vishwanath, et al., *Phys. Rev. B* **83**, 205101 (2011).
<https://doi.org/10.1103/PhysRevB.83.205101>
12. Binghai Yan and C. Felser, *Annu. Rev. Condens. Matter. Phys.* **8**, 337 (2017).
<https://doi.org/10.1146/annurev-conmatphys-031016-025458>
13. N. P. Armitage, E. J. Mele, and A. Vishwanath, *Rev. Mod. Phys.* **90**, 015001 (2018).
<https://doi.org/10.1103/RevModPhys.90.015001>
14. M. M. Otrokov, I. I. Klimovskikh, H. Bentmann, et al., *Nature* **576**, 416 (2019).
<https://doi.org/10.1038/s41586-019-1840-9>
15. A. M. Shikin, D. A. Estyunin, I. I. Klimovskikh, et al., *Sci. Rep.* **10**, 13226 (2020).
<https://doi.org/10.1038/s41598-020-70089-9>
16. A. M. Shikin, T. P. Makarova, A. V. Eryzhenkov, et al., *Phys. B. Condens. Matter.* **649**, 414443 (2023).
<https://doi.org/10.1016/j.physb.2022.414443>
17. A. M. Shilkin, N. L. Zaitsev, A. V. Tarasov, et al., *JETP Lett.* **116**, 556 (2022).
<https://doi.org/10.1134/S0021364022601890>
18. A. M. Shilkin, D. A. Estyunin, D. A. Glazkova, et al., *JETP Lett.* **115**, 213 (2022).
<https://doi.org/10.1134/S0021364022040117>
19. D. A. Glazkova, D. A. Estyunin, I. I. Klimovskikh, et al., *JETP Lett.* **115**, 286 (2022).
<https://doi.org/10.1134/S0021364022340057>
20. A. M. Shikin, D. A. Estyunin, N. L. Zaitsev, et al., *Phys. Rev. B* **104**, 115168 (2021).
<https://doi.org/10.1103/PhysRevB.104.115168>
21. M. Garnica, M. M. Otrokov, P. Casado Aguilar, et al., *npj Quantum Mater.* **7** (7) (2022).
<https://doi.org/10.1038/s41535-021-00414-6>
22. Yu-Jie Hao, Pengfei Liu, Yue Feng, et al., *Phys. Rev. X* **9**, 041038 (2019).
<https://doi.org/10.1103/PhysRevX.9.041038>
23. S. V. Eremeev, I. P. Rusinov, Yu. M. Koroteev, et al., *J. Phys. Chem. Lett.* **12**, 4268 (2021).
<https://doi.org/10.1021/acs.jpcllett.1c00875>
24. J.-Q. Yan, Q. Zhang, T. Heitmann, et al., *Phys. Rev. Mater.* **3**, 064202 (2019).
<https://doi.org/10.1103/PhysRevMaterials.3.064202>
25. Bing Li, J.-Q. Yan, D. M. Pajerowski, et al., *Phys. Rev. Lett.* **124**, 167204 (2020).
<https://doi.org/10.1103/PhysRevLett.124.167204>
26. A. Zeugner, F. Nietschke, A. U. B. Wolter, et al., *Chem. Mater.* **31**, 2795 (2019).
<https://doi.org/10.1021/acs.chemmater.8b05017>
27. D. A. Estyunin, I. I. Klimovskikh, A. M. Shikin, et al., *APL Mater.* **8**, 021105 (2020).
<https://doi.org/10.1063/1.5142846>
28. C. Lei, O. Heinonen, A. H. MacDonald, et al., *Phys. Rev. Mater.* **5**, 064201 (2021).
<https://doi.org/10.1103/PhysRevMaterials.5.064201>
29. Wenbo Ge, Jinwoong Kim, Ying-Ting Chan, et al., *Phys. Rev. Lett.* **129**, 107204 (2022).
<https://doi.org/10.1103/PhysRevLett.129.107204>
30. I. M. Band, Yu. I. Kharitonov, and M. B. Trzhaskovskaya, *At. Data Nucl. Data Tables* **23**, 443 (1979).
[https://doi.org/10.1016/0092-640X\(79\)90027-5](https://doi.org/10.1016/0092-640X(79)90027-5)
31. P. Rani, A. Saxena, R. Sultana, et al., *J. Supercond. Nov. Magn.* **32**, 3705 (2019).
<https://doi.org/10.1007/s10948-019-05342-y>
32. A. S. Borovik-Romanov, N. M. Kreines, A. A. Pankov, et al., *JETP Lett.* **37**, 890 (1973).
33. V. Saidl, P. Nemeč, P. Wadley, et al., *Nat. Photon.* **11**, 91 (2017).
<https://doi.org/10.1038/nphoton.2016.255>
34. Kexin Yang, Kisung Kang, Zhu Diao, et al., *Phys. Rev. Mater.* **3**, 124408 (2019).
<https://doi.org/10.1103/PhysRevMaterials.3.124408>
35. I. I. Klimovskikh, M. M. Otrokov, D. A. Estyunin, et al., *npj Quantum Mater.* **5**, 54 (2020).
<https://doi.org/10.1038/s41535-020-00255-9>
36. Chaowei Hu, Shang-Wei Lien, Erxi Feng, et al., *Phys. Rev. B* **104**, 054422 (2021).
<https://doi.org/10.1103/PhysRevB.104.054422>
37. Bo Chen, Fucong Fei, Dongqin Zhang, et al., *Nat. Commun.* **10**, 4469 (2019).
<https://doi.org/10.1038/s41467-019-12485-y>
38. D. A. Glazkova, D. A. Estyunin, I. I. Klimovskikh, et al., *JETP Lett.* **116**, 817 (2022).
<https://doi.org/10.1134/S0021364022602445>
39. Yaohua Liu, Lin-Lin Wang, Qiang Zheng, et al., *Phys. Rev. X* **11**, 021033 (2021).
<https://doi.org/10.1103/PhysRevX.11.021033>

Translated by A. Sin'kov

Publisher's Note. Pleiades Publishing remains neutral with regard to jurisdictional claims in published maps and institutional affiliations.